Influence of coil current modulation on TiO2 nanoparticle synthesis using pulse-modulated induction thermal plasmas

Influence of coil current modulation on TiO_2 nanoparticle synthesis using pulse-modulated induction thermal plasmas

Y. Tanaka[a], H. Sakai[a], T. Tsuke[a], Y. Uesugi[a], Y. Sakai[b], K. Nakamura[b]

[a] *Faculty of Electrical and Computer Engineering, Kanazawa University, Kakuma, Kanazawa 920-1192, Japan*
[b] *Powder Technol. & Res. Sec., Nisshin Seifun Gr. Inc., 5-3-1 Tsurugaoka, Fujimino 356-8511, Japan*

Abstract

This paper describes the relation between the size of synthesized nanoparticles and the temperature variation of the surrounding plasma in TiO_2 nanoparticle synthesis using pulse-modulated induction thermal plasmas (PMITP). The Ar-O_2 PMITP at 20 kW was used to obtain repetitional temperature fields at pressure of 200 Torr. The TiO_2 nanoparticles were synthesized by direct injection of Ti powder with mean diameter of 45 μm. Dependence of the nanoparticle size on modulation parameters such as the duty factor and the shimmer current level of the PMITP were investigated experimentally. Instantaneous temperature evolution was evaluated through spectroscopic observation. Experimental results show that the temperature decay rate in the PMITP reached 10^5–10^6 K/s, and that the mean diameter of synthesized particles decreased with the temperature decay rate.

Keywords: Nanoparticle, Titanium dioxide, Thermal plasma, High-pressure plasma,

1. Introduction

Inductively coupled thermal plasmas (ICTPs) operating at several tens of kilowatts are widely used for various material processes such as syntheses of diamond films [1], thermal barrier coatings [2], syntheses of fullerene [3], materials surface modifications [4], and nanoparticle syntheses [5, 6, 7].For example, titanium dioxide (TiO_2) nanoparticles have attracted much interest for various applications such as photocatalysts [8], photonic crystals [9], photovoltaic cells [10], and gas sensors [11]. The synthesis of TiO_2 nanoparticles has therefore been investigated in many research efforts using a steady-state type of ICTP [6, 7].

We have developed some high-power modulated induction thermal plasma systems, known as PMITP and AMITP [12, 13]. The pulse-modulated induction thermal plasma (PMITP) system can modulate the coil current sustaining the induction thermal plasma into a rectangular waveform. It can change the temperature and radical densities as well as the gas flow field in the thermal plasma in a time domain [12]. Some studies have tried to adopt the PMITP for surface modification of materials using good controllability of the temperature and radical densities [14, 15, 16] A high-power arbitrary-waveform-modulated induction thermal plasma (AMITP) system has also been developed for additional enhancement of the degrees of freedom in thermal plasma control [13]. The AMITP system can modulate the coil current not only into a rectangular waveform but also into an externally given waveform, which provides precise time-domain control of the temperature of thermal plasmas [13].

We have started studying nanoparticle synthesis using a modulated induction thermal plasma [17]. The two following main effects can be expected in nanoparticle syntheses using modulated thermal plasmas. One is rapid and complete evaporation of injected raw materials during high-power input time duration, with subsequent rapid cooling of the evaporated material during the low-power input period. In particular, the low-power input period in the modulation might provide rapid cooling of the evaporated material, which can be described as the temperature decay rate $|\partial T/\partial t|$. This temperature decay rate $|\partial T/\partial t|$ is expected to be of 10^5–10^6 K/s order in the PMITP, in addition to the temperature history of the evaporated material by convection $|\boldsymbol{u} \cdot \nabla T|$, where T is the temperature, t is the time, and $\boldsymbol{u}$ is the gas flow vector. In other words, we anticipate that the temperature history of evaporated material $|dT/dt|$ is $|\partial T/\partial t + \boldsymbol{u} \cdot \nabla T|$. The rapid temperature history of

10^5–10^6 K/s for evaporated material is known to be useful to create nanoparticle synthesis [18, 19]. The other is the enhancement of the time-averaged temperature-gradient, which also causes cooling of evaporated material during transfer to the downstream chamber. It is related with $|\boldsymbol{u} \cdot \nabla T_{\mathrm{ave}}|$, where T_{ave} is the average temperature. This enhancement of the time-averaged temperature gradient has been observed also in other applications of the PMITP in experiments and numerical simulations conducted in our previous works [15, 20]. Actually, our previous study related to nanoparticle synthesis using PMITP [17], revealed that the higher degree of the coil current modulation for the PMITP can provide smaller TiO_2 nanoparticles at a fixed duty factor (DF) of 80%, and that the weight fraction of anatase-TiO_2 nanoparticles to the synthesized particles were 80–90%, almost irrespective of the modulation degree. In addition, our estimation of the time-averaged temperature in the reaction chamber revealed that the time-averaged temperature was decreased by the modulation of the coil current even at the same input power of 20 kW used in our previous study. However, the effect of current modulation for different duty factors and the instantaneous temperature variation have been not yet investigated.

This paper describes the influence of modulation conditions such as the duty factor (DF) and the shimmer current level (SCL) on TiO_2 nanoparticle synthesis using Ar-O_2 PMITP at 20 kW. For this purpose, 15 combinations of DF and SCL were experimentally studied to assess their effects on the mean particle size and the weight fraction of synthesized nanoparticles. Furthermore, the time evolution in the temperature of the thermal plasma in the reaction chamber was determined using time resolution spectroscopic observation to investigate rapid changes in the temperature. Based on the temperature measurement results, the relation between the temperature decay rate during the low input-power duration and the mean diameter of synthesized nanoparticles was obtained to investigate instantaneous rapid cooling effects of evaporated material. The main contribution of this paper is the experimental confirmation of the pulse modulation effect on nanoparticle synthesis.

2. Experimental

2.1. Experimental arrangements

Fig. 1 depicts the experimental setup and the details of this setup can be found in our previous paper [17]. We used a radio frequency (rf) power

supply with a metal-oxide semiconductor field emission transistor (MOSFET). It can also modulate electric current of several hundreds of amperes for supplying the coil current. The amplitude of the coil current sustaining induction thermal plasmas was modulated into a rectangular waveform in this work. The modulated coil current has modulation parameters such as the shimmer current level (SCL), the on-time, and the off-time [12]. Fig. 2 presents a definition of the modulation parameters. The 'on-time' is defined as the time duration with higher current level (HCL); the 'off-time' is the time duration with lower current level (LCL). The shimmer current level is defined as a ratio of the lower current level (LCL) to the higher current level (HCL). In addition, the duty factor (DF) is set to a ratio of the on time to one modulation cycle: DF= 'on-time' /('on-time' +'off-time'). Either condition 100%SCL or 100%DF corresponds to the non-modulation condition. Conditions SCL<100% and DF<100% provide a modulation condition. Lower SCL engenders a larger modulation. Synthesized particles were collected in the upstream chamber, the downstream chamber, and in the filter.

2.2. Experimental conditions

The total flow rate of Ar-O_2 sheath gas was fixed at 80.0 standard liters per minute (slpm) (=1.33 $\times$ 10^{-3} m^3 s^{-1}). The oxygen gas admixture ratio to Ar was 10% in the sheath gas in the gas flow rate. The gas flow rate of Ar carrier gas was 2 slpm. Titanium powder with mean diameter of 45 μm is fed as the raw material. The powder feed rate g of the Ti raw material was fixed at around 3.5 g min^{-1} to 4.0 g min^{-1} (= 5.8 $\times$ 10^{-5} kg s^{-1} to 6.7 $\times$ 10^{-5} kg s^{-1}). The pressure inside the chamber was controlled at 300 Torr (=40 kPa) with an automatic feedback control for pressure.

In this work, we fixed the input power of 20 kW to the inverter power supply irrespective of the modulation condition. In this case, the HCL and the LCL were experimentally adjusted for the time-averaged input power in a modulation cycle to be 20 kW. On the other hand, the modulation cycle was fixed at 15 ms in the present work because the residence time of the reactant vapor was estimated as 10–20 ms [17]. It is expected to provide sufficient evaporation of the injected powders in the high-temperature region in the plasma during the on-time, and successive rapid cooling of the plasma tail during the off-time.

Combination of DF and SCL affects the temperature and gas flow fields of the PMITP. However, reducing DF or reducing SCL causes a greater disturbance in the PMITP, which can cause extinction of the PMITP. Therefore,

a stable operation region of the PMITP exists for the combination of DF and SCL. Fig. 3 presents the experimentally obtained stable operation region of Ar-O_2 PMITP at 20 kW for different DFs and SCLs. The circles in this figure represent the combinations of DF and SCL with which the Ar-O_2 PMITP could be established; the crosses denote the combination of DF and SCL with which the Ar-O_2 PMITP was extinguished. From this figure, 15 combinations of DF and SCL in the modulation were set for experiments for synthesis of nanoparticles as presented in Table 1.

3. Influence of current modulation on synthesized particles

3.1. SEM images and mean diameters

Fig. 4 presents examples of FE-SEM micrographs of particles synthesized using induction thermal plasma with and without the coil current modulation. Panel (a) portrays the image for DF=100%, i.e. a non-modulation condition, whereas panels (b)–(e) portray images for different DFs. For all images, the SCL was fixed at 80%. As might be readily apparent, reducing DF from 100%–67% roughly increases the particle size. In contrast, reducing DF from 67%–60% seems to increase the particle size approximately. The influences of DF and SCL on the mean diameter of synthesized particles were summarized completely for given 15 experimental conditions in Fig. 5. The error bars include fluctuations from three experiments for the fixed condition. The mean particle diameter was evaluated by measuring diameters of randomly selected 200 particles in each of the SEM micrograph images. This figure shows that reducing SCL provides smaller nanoparticles for DFs from 90%–67%, especially at 80%DF among the tested combinations of DF and SCL. This decrease in the particle size implies that the coil current modulation causes more rapid cooling of evaporated material than that with no modulation. This rapid cooling effect will be discussed in a later section of the temperature evolution of the PMITP. On the other hand, at DF=60%, the mean particle diameter hardly decreased with reducing SCL. Furthermore, reducing DF from 67% to 60% provides larger nanoparticles. This increase in the particle size might result from the fact that the amplitude of temperature change of the PMITP in the plasma torch is lower at small DF because of the short on-time. Therefore, a rapid temperature change might not be obtained in the reaction chamber. Explanation of this phenomenon demands future work on the quenching phenomena of evaporated material in the PMITP.

3.2. XRD spectra and fraction of anatase

The crystallographic structure and chemical composition of the synthesized nanoparticles were investigated using X-ray diffraction (XRD) analysis. Almost identical XRD spectra were obtained for all particles synthesized using PMITP with different DFs. Calculating the ratio of the XRD intensity for these spectral lines, we estimated the weight fraction f_{A} of TiO_2 in anatase form to TiO_2 in rutile form using the method indicated in [7, 17]. Fig. 6 presents the weight fraction of anatase TiO_2 to rutile TiO_2 as a function of SCL for different DFs. The weight fraction of anatase TiO_2 remains at 0.8–0.9, almost irrespective of DF and SCL. The unchanged weight fraction shows that the PMITP continues to provide sufficient higher temperature-quenching at the plasma tail region for nucleation of anatase TiO_2 for different modulation conditions because nucleation of anatase TiO_2 tends to occur around 2075 K by higher degrees of undercooling of molten materials according to a theoretical calculation of the critical free energy for nucleation of rutile and anatase TiO_2 reported in the literature [21].

3.3. Time evolution in temperature during nanoparticle synthesis

3.3.1. Observation of time evolution in emission spectra

As described previously, we anticipate the following two effects in nanoparticle syntheses in a PMITP. One effect is the enhancement of time-averaged temperature gradient, which causes cooling of the evaporated material during its transfer to the downstream chamber by convection. This enhancement of the time-averaged temperature gradient was investigated in our previous paper [17]. We found that the modulation causes the time-averaged temperature decreased in the reaction chamber. The other effect is rapid evaporation of the injected raw material during the on-time and its rapid cooling during off-time. In particular, rapid cooling can influence the synthesis of nanoparticles.

To study the time evolution of the PMITP in the reaction chamber where nanoparticles can be created, spectroscopic observation was conducted there using a time-resolution measurement with a polychromator as indicated in Fig. 1. The observation position was set at 200 mm below the coil end. The observation spot was about 8 mm in diameter. The polychromator has an observation wavelength range of 300–1200 nm with a wavelength resolution of 1 nm. Details of the observation system can be referred from our previous paper [17]. In the present work, the exposure time of the ICCD used here was set to 100 μs.

Fig. 7 shows the time evolution in the observed emission spectra at wavelengths of 400–850 nm. Panel (a) in that figure shows spectra for a non-modulated thermal plasma; panel (b) shows spectra for PMITP with 80%DF-70%SCL. These spectra are shown t=0, 3, 6, 9, 12, and 15 ms after the current transition from LCL to HCL. Atomic spectral lines of Ar, Ti, and O, and molecular spectra of TiO are visible in both non-modulation and modulation cases. In the non-modulation case, there is little time change in the radiation intensity of these observed spectra. On the other hand, in the modulation case, the radiation intensity of the observed spectra changed greatly following the modulation cycle. The respective time evolutions in the radiation intensity of these spectra are similar, irrespective of the species. This similarity reflects that the observed change in the radiation intensity arises mainly from change in the bulk plasma, for example, by a change in the temperature. The temperature mentioned here seems rather the electronic excitation temperature because the radiation intensities of both molecular spectra and also atomic spectra change similarly and largely with the coil current modulation. The electronic excitation temperature are considered close to the electron temperature T_{e} since the electronic excitation of species occurs mainly by electron impact. The T_{e} has a fast response to the joule heating from electric field created by the coil current. Thus, the electronic excitation temperature changes following the coil current modulation, and then the radiation intensities for each of species similarly modulated as indicated in Fig. 7(b). It was also obtained that reducing SCL causes a larger change in the radiation intensity of TiO molecular spectra, which might indicate that reducing SCL, which means a larger modulation, produces a larger temperature change in the PMITP in the reaction chamber.

3.3.2. Time evolution in vibrational and rotational temperatures of TiO

Time evolution in the vibrational temperature T_{vib} and the rotational temperature T_{rot} of TiO were determined by fitting the theoretically calculated radiation intensity of TiO spectra to that of the experimentally measured TiO spectra. Calculation procedures such as the theory and the convolution technique were described in our previous paper [17]. It is noteworthy that the T_{rot} and T_{vib} estimated here are based on the radiation intensity integrated along the line of sight with no Abel inversion. Consequently, the estimated T_{rot} and T_{vib} are only approximation temperatures for them. In spite of this fact, T_{vib} is also considered close to the T_{e} because the vibrational excitation mainly occurs by electron impact according to the order estima-

tion of vibrational excitation reaction rates for electron and heavy particle collisions. On the other hand, T_{rot} is close to the gas temperature T_{h} because of high rotational excitation rate by heavy particle collisions. Therefore, we can estimate time evolution in T_{e} and T_{h}.

Fig. 8 presents the time evolution in T_{vib} and T_{rot} observed at 200 mm below the coil end in the PMITP for SCL=70% DF=80%. This figure includes the T_{rot} for the no modulation condition, which was estimated as about 4500 K. The value of T_{vib} for the no modulation condition was also estimated as 5500 K. It is noticed that the time-averaged T_{vib} and T_{rot} for the modulation condition in Fig. 8 are lower than those without modulation. These lower time-averaged T_{vib} and T_{rot} were also found in our previous work [17]. Immediately after current transition from LCL to HCL, i.e. around t=0 ms, the T_{vib} rapidly increases from 3700 to 4700 K. This rapid increase in T_{vib} results from a rapid increase in the T_{e} because T_{e} drastically increased as a result of the rapid increase in the electric field. Following this increase in the T_{vib}, the T_{rot} is increased. After that around t=2.5 ms, T_{vib} decreases approaching T_{rot}. At t=12 ms, where a current transition exists from HCL to LCL, T_{vib} decreases rapidly. On the other hand, T_{rot} increases slightly in this time, then decreases during the off-time. This temporary increase in T_{rot} just after the transition HCL to LCL might be attributable to the reaction heat by association of Ti and O during the off-time. Conversely, if there was not such association reactions, T_{rot} might be monotonously decreased in the off-time since the input power to the plasma decreases. The association reaction heat might be transferred to translational and rotational energy of TiO molecules.

3.3.3. Relation between the temperature decay rate and nanoparticle size

For nanoparticle synthesis, the gas temperature T_{h}, which is close to T_{rot}, might mainly influence nucleation, condensation, and coagulation mechanisms. We therefore estimated the decay rate in the T_{rot}, which is designated by $|\partial T_{\mathrm{rot}}/\partial t|$, from the determined time evolution in T_{rot} during the off-time for different DFs and SCLs. Fig. 9 shows the experimentally obtained relation between $|\partial T_{\mathrm{rot}}/\partial t|$ and the mean diameter of synthesized nanoparticles. As the figure shows, a relation can be found between $|\partial T_{\mathrm{rot}}/\partial t|$ and the mean diameter. This figure shows that $|\partial T_{\mathrm{rot}}/\partial t|$ reaches 10^5–10^6 K/s, and that increasing $|\partial T_{\mathrm{rot}}/\partial t|$ provides smaller nanoparticles. Therefore, PMITP can engender a higher $|\partial T_{\mathrm{rot}}/\partial t|$. That higher $|\partial T_{\mathrm{rot}}/\partial t|$ definitely provides smaller nanoparticles.

According to the literature [21], the metastable anatase-TiO_2 is formed below 2075 K under higher cooling rate. This nucleation temperature of 2075 K is lower than the $T_{\rm rot}$ estimated here. In spite of that, we infer that a higher $|\partial T_{\rm rot}/\partial t|$ estimated here links a higher temperature decay rate around the nucleation temperature of anatase-TiO_2, and then that it provides smaller nanoparticles of anatase-TiO_2.

4. Conclusions

In summary, a 20 kW class of Ar-O_2 pulse-modulated induction thermal plasma (PMITP) was used for synthesis of TiO_2 nanoparticles for different modulation conditions including those of the shimmer current level and duty factor. Experimental results show that a modulation condition of 80%DF-65%SCL provides smaller nanoparticles among 15 combinations of DF and SCL, and that the weight fraction of anatase TiO_2 in the synthesized particles was estimated as 80%–90%, almost independent of the modulation condition in the coil current. Additionally, results show that that a larger modulation causes a large temperature change in the PMITP, which might provide smaller nanoparticles. Therefore, PMITP can engender a higher $|\partial T_{\rm rot}/\partial t|$. That higher $|\partial T_{\rm rot}/\partial t|$ definitely provides smaller nanoparticles.

References

[1] J.O. Berghaus, J.L. Meunier, F. Gitzhofer, Monitoring and control of RF thermal plasma diamond deposition via substrate biasing, Meas. Sci. Technol. 15 (2004) 161–164.

[2] W.R. Chen, X. Wu, B.R. Marple, P.C. Patnaik, Oxidation and crack nucleation/growth in an air-plasma-sprayed thermal barrier coating with NiCrAly bond coat, Surface & Coatings Technol. 197 (2005) 109–115.

[3] C. Wang, A. Inazaki, T. Shirai, Y. Tanaka, T. Sakuta, H. Takikawa, H. Matsuo, Effect of ambient gas and pressure on fullerene synthesis in induction thermal plasma, Thin Solid Films 425 (2003) 41–48.

[4] H. Tanaka, T. Osawa, Y. Moriyoshi, M. Kurihara, S. Maruyama, T. Ishigaki, Improvement of the anode performance of graphite particles through surface modification in RF thermal plasma, Thin Solid Films 457 (2004) 209–216.

[5] M. Shigeta, T. Watanabe, H. Nishiyama, Numerical investigation for nano-particle synthesis in an RF inductively coupled plasma, Thin Solid Films 457 (2004) 192–200.

[6] J.E. Lee, S.M. Oh, D.W. Park, Synthesis of nano-sized Al doped TiO_2 powders using thermal plasma, Thin Solid Films 457 (2004) 230–234.

[7] J.G. Li, M. Ikeda, R. Ye, Y. Moriyoshi, T. Ishigaki, Control of particle size and phase formation of TiO_2 nanoparticles synthesized in RF induction plasma, J. Phys. D: Appl. Phys. 40 (2007) 2348–2353.

[8] S. Malato, J. Blanco, D. C. Alarcon, M.I. Maldonado, P. Fernandez-Ibanez, W. Gernjak, Photocatalytic decontamination and disinfection of water with solar collectors, Catalysis Today 122 (2007) 137–49.

[9] J. Li, X. Zhao, H. Wei, Z.Z. Gu, Z. Lu, Macroporous ordered titanium dioxide (TiO_2) inverse opal as a new label-free immunosensor, Analytica Chemica Acta 625 (2008) 63–69.

[10] M. Gratzel, Photoelectrochemical cells, Nature 414 (2001) 338–344.

[11] K.P. Biju, M.K. Jain, Effect of crystallization on humidity sensing properties of sol-gel derived nanocrystalline TiO_2 thin films, Thin Solid Films 516 (2008) 2175–2180.

[12] Y. Tanaka, Y. Uesugi, T. Sakuta, Controlling the number of excited atoms flowing into the reaction chamber using pulse-modulated induction thermal plasmas at atmospheric pressure, Plasma Sources Sci. & Technol. 16 (2007) 281–289.

[13] Y. Tanaka, Y. Morishita, K. Okunaga, S. Fushie, Y. Uesugi, Generation of high-power arbitrary-waveform modulated inductively coupled plasmas for materials processing, Appl. Phys. Lett. 90 (2007) 071502.

[14] N. Ohashi, Y. G. Wang, T. Ishigaki, Y. Wada, H. Taguchi, I. Sakaguchi, T. Ohgaki, Y. Adachi, H. Haneda, Lowered stimulated emission threshold of zinc oxide by hydrogen doping with pulsed argon–hydrogen plasma, J. Crystal Growth 306 (2007) 316–320.

[15] Y. Tanaka, T. Muroya, K. Hayashi, Y. Uesugi, Simultaneous control of numerical enhancement of N atom and decrease in heat flux into reaction chamber, using Ar-N_2 pulse-modulated induction thermal plasmas, Appl. Phys. Lett. 89 (2006) 031501.

[16] Y. Tanaka, T. Muroya, K. Hayashi, Y. Uesugi, Control of nitrogen atomic density and enthalpy flow into reaction chamber in Ar-N_2 pulse-modulated induction thermal plasmas, IEEE Trans. Plasma Sci. 35 (2007) 197–203.

[17] Y. Tanaka, T. Nagumo, H. Sakai, Y. Uesugi, Y. Sakai, K. Nakamura, Nanoparticle synthesis using high-powered pulse-modulated induction thermal plasmas, J. Phys. D: Appl. Phys. 43 (2010) 2010.

[18] P.C. Kong, Y.C. Lau, Plasma synthesis of ceramic powders, Pure & Appl. Chem. 62 (1990) 1809–1816.

[19] T. Ishigaki, J.-G. Li, M. Ikeda, H. Kamiyama, R. Ye, X.H. Wang, M. Moriyoshi, Proc. of 8th Asia-Pacific Conf. Plasma Sci.& Technol., Cairns, Australia, p. 112. 6.

[20] R. Ye, A.B. Murphy, T. Ishigaki, Numerical modeling of an Ar-H_2 radio-frequency plasma reactor under thermal and chemical nonequilibrium conditions, Plasma Chem. & Plasma Process. 27 (2007) 189–204.

[21] Y. Li, T. Ishigaki, Thermodynamic analysis of nucleation of anatase and rutile from TiO_2 melt, J. Cryst. Growth, 242 (2002) 511–516.

Table 1: Experimental condition.

No.	SCL [%]	DF [%]	On-time/Off-time [ms]/[ms]	Ti powder feed rate [mg/s]
1	100	100	-	3.35
2	90	90	13.5/1.5	3.56
3	80	90	13.5/1.5	3.54
4	70	90	13.5/1.5	3.52
5	65	90	13.5/1.5	3.48
6	62	90	13.5/1.5	3.58
7	90	80	12.0/3.0	4.06
8	80	80	12.0/3.0	3.92
9	70	80	12.0/3.0	3.43
10	65	80	12.0/3.0	3.56
11	90	67	10.0/5.0	3.74
12	80	67	10.0/5.0	3.48
13	70	67	10.0/5.0	3.61
14	90	60	9.0/6.0	3.62
15	80	60	9.0/6.0	3.94

Table captions

1. Experimental condition.

Figure captions

1. Experimental setup for nanoparticle synthesis.
2. Modulated coil current and definition of modulation parameters.
3. Stable operation region of Ar-O_2 PMITP at 20 kW.
4. SEM micrographs of synthesized particles collected in the filter: (a) w/o modulation (100%SCL), (b) 90%DF-80%SCL, (c) 80%DF-80%SCL, (d) 67%DF-80%SCL, and (e) 60%DF-80%SCL.
5. Dependence of the mean diameter of synthesized particles on the duty factor (DF) for different shimmer current levels (SCL) in modulated coil current.
6. Dependence of the weight fraction of anatase-TiO_2 nanoparticles on the shimmer current level (SCL) at different duty factors (DF) in modulated coil current.
7. Time evolution in emission spectra observed at 200 mm below the coil end in the reaction chamber installed downstream of the plasma torch during feeding Ti raw powder. (a) w/o modulation, (b) w/ modulation of 80%DF-70%SCL.
8. Time evolution in vibrational and rotational temperature of TiO at 200 mm below the coil end in PMITP at 80%DF-70%SCL.
9. Relation between the mean diameter of synthesized nanoparticles and the decay rate of rotational temperature

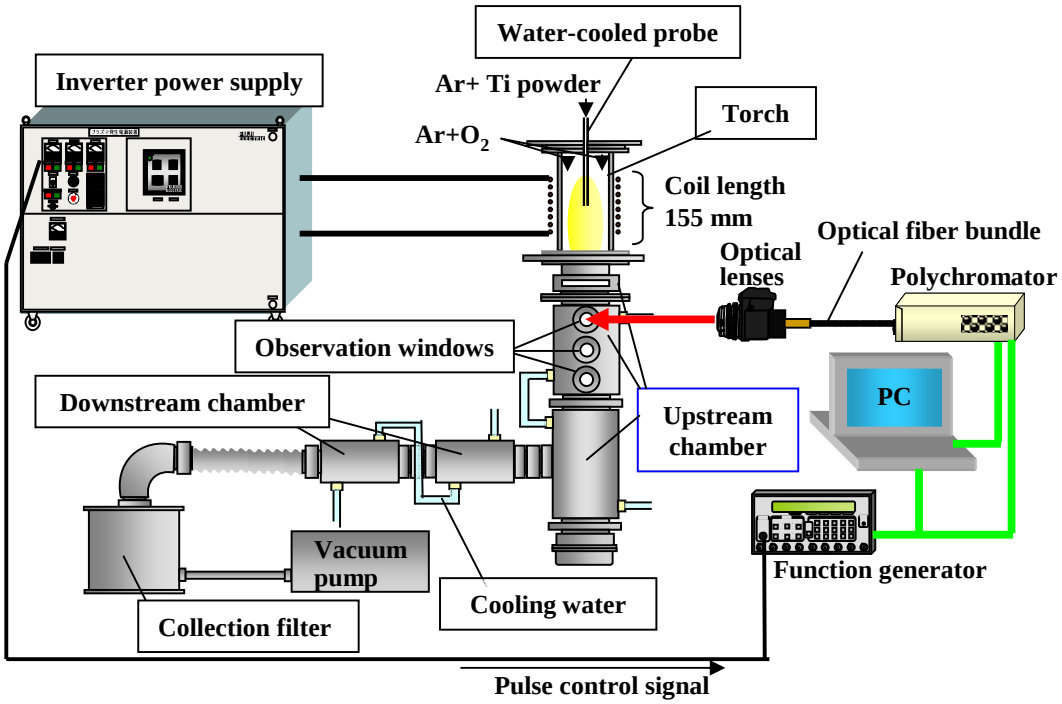

Figure 1: Experimental setup for nanoparticle synthesis.

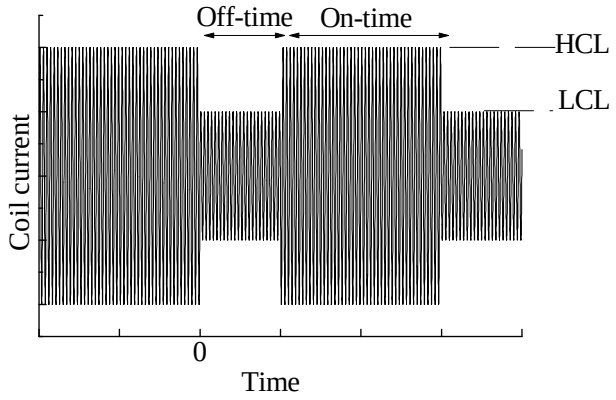

Figure 2: Modulated coil current and definition of modulation parameters.

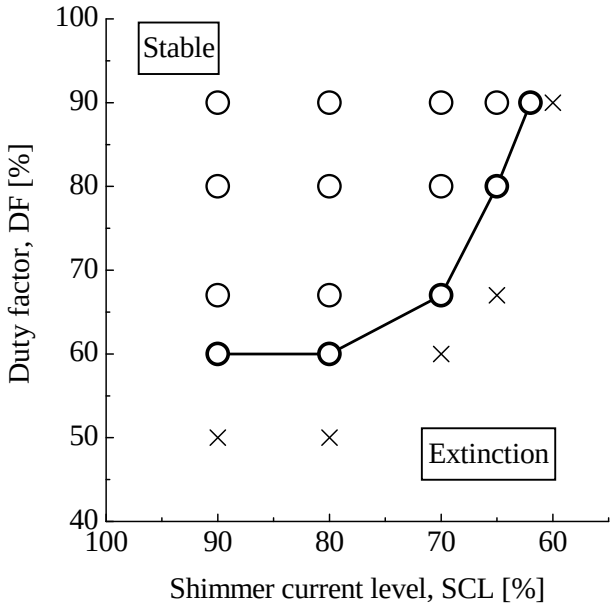

Figure 3: Stable operation region of Ar-O_2 PMITP at 20 kW.

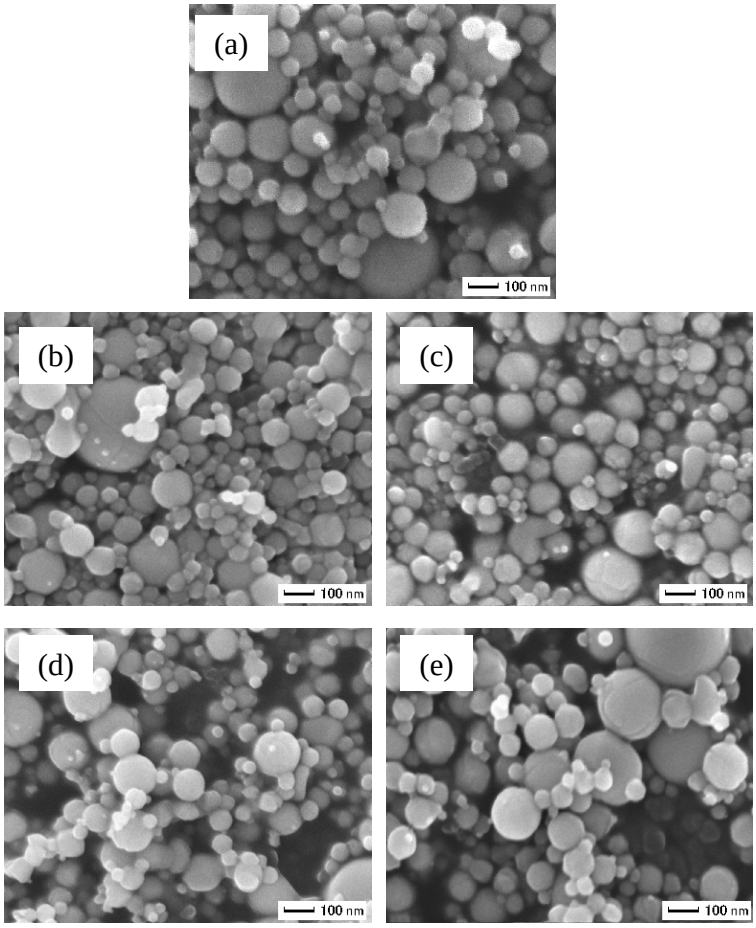

Figure 4: SEM micrographs of synthesized particles collected in the filter: (a) w/o modulation (100%SCL), (b) 90%DF-80%SCL, (c) 80%DF-80%SCL, (d) 67%DF-80%SCL, and (e) 60%DF-80%SCL.

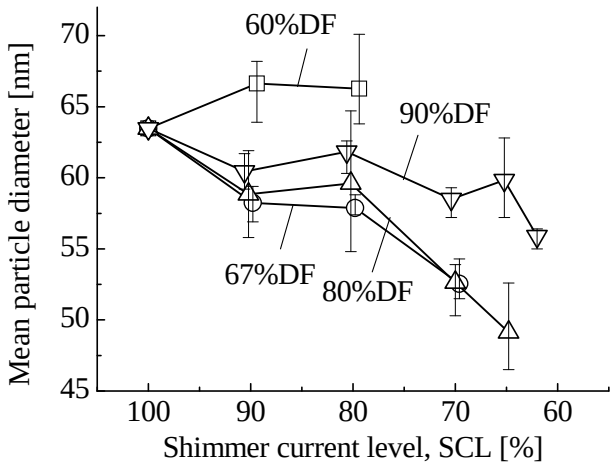

Figure 5: Dependence of the mean diameter of synthesized particles on the duty factor (DF) for different shimmer current levels (SCL) in modulated coil current.

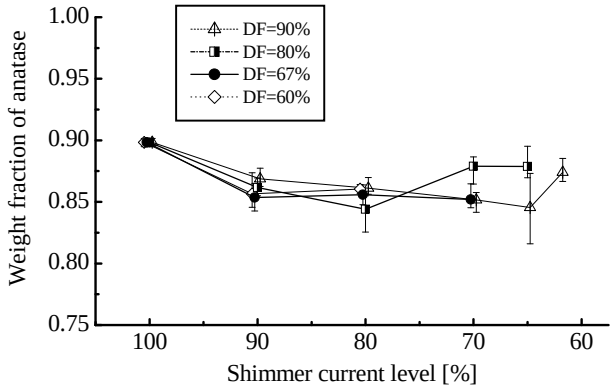

Figure 6: Dependence of the weight fraction of anatase-TiO_2 nanoparticles on the shimmer current level (SCL) at different duty factors (DF) in modulated coil current.

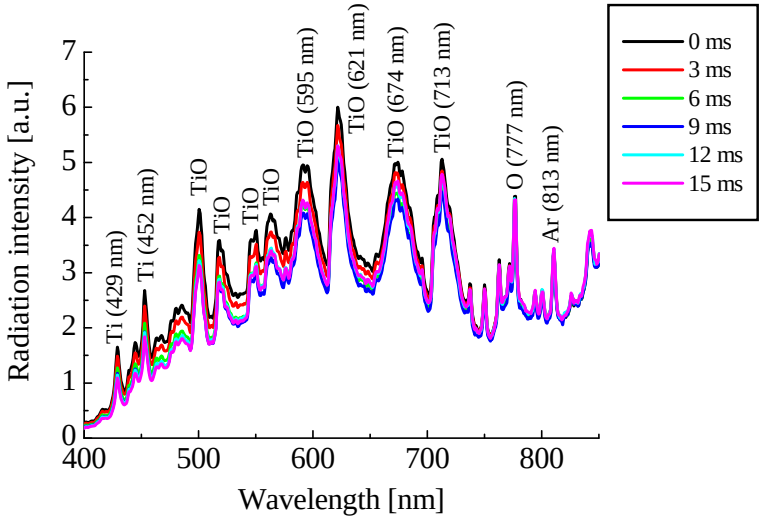

(a) w/o modulation.

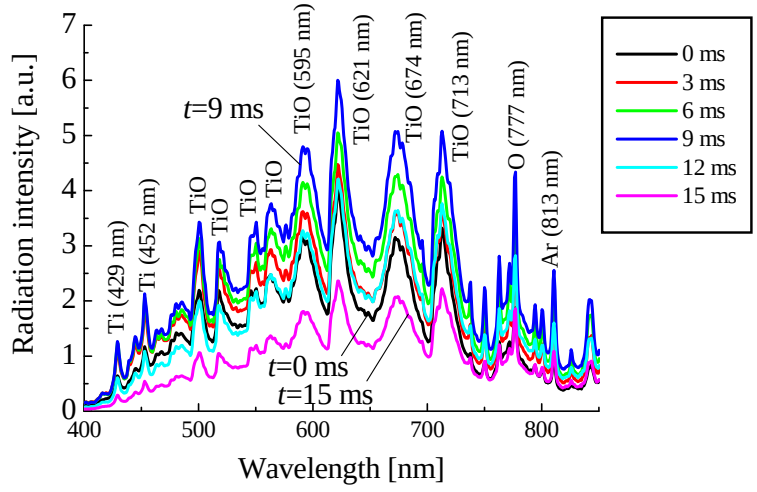

(b) w/ modulation.
(67%DF-80%SCL. Ontime=10 ms, Off-time=5 ms).

Figure 7: Time evolution in emission spectra observed at 200 mm below the coil end in the reaction chamber installed downstream of the plasma torch during feeding Ti raw powder. (a) w/o modulation, (b) w/ modulation of 80%DF-70%SCL.

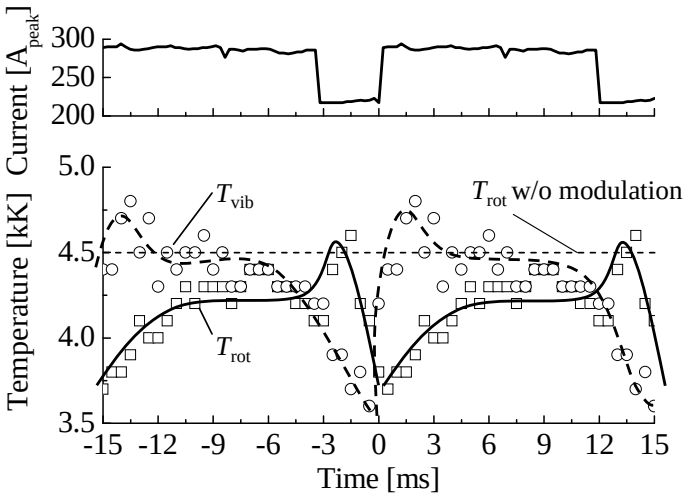

Figure 8: Time evolution in vibrational and rotational temperature of TiO at 200 mm below the coil end in PMITP at 80%DF-70%SCL.

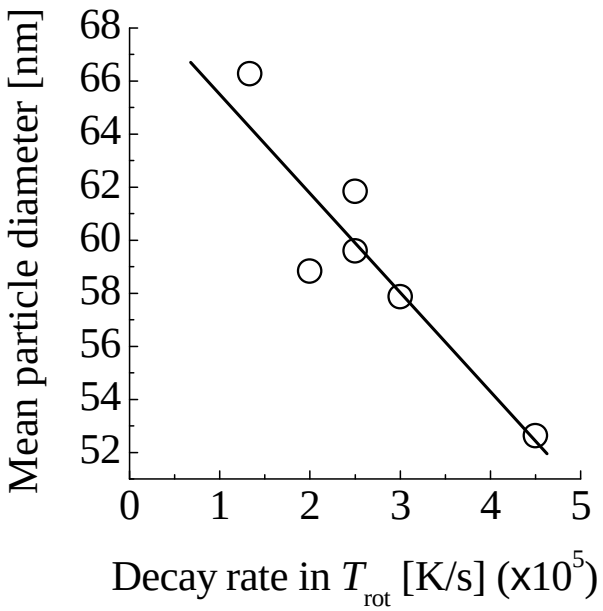

Figure 9: Relation between the mean diameter of synthesized nanoparticles and the decay rate of rotational temperature